IRANIAN JOURNAL OF PHYSICS RESEARCH

Iranian Journal of Physics Research, Vol. 23, No. 3, 2023
DOI: 10.47176/ijpr.22.3.61501

Enhancement of spontaneous emission and material gain from CdSe/CdS quantum dot

K R Ghadeer and J Jamal Nasir
Physics Department ,College of Education , University of Al-Qadisiyah , Diwaniyah , Iraq

E-mail: jamal.jabir@qu.edu.iq

(Received 27 June 2022 ; in final form 14 June 2023)

Abstract
This study looks at the material gain and enhanced spontaneous emission of CdSe(1-x)S(x)/ZnS and CdSe(1-x)S(x)/ZnO quantum dot (QD) structures. (remove dot) cadmium selenide (CdSe) QDs, cadmium sulfide (CdS) wetting layer (WL), zinc oxide (ZnO) and zinc sulfide (ZnS) as a barrier layers were investigated to achieve QDs semiconductor with active region (B). The energy levels and band alignment between layers are predicted using the quantum disk model. Gain is an estimation for the transverse electric (TE) and magnetic (TM) modes in QDs structures, taking into consideration the momentum matrix element. The mole-fraction (x) and contributions of the barriers (ZnO and ZnS) material in enhanced gain and spontaneous emission were investigated in this manuscript. When ZnS is used as a barrier material, the spontaneous emission is found to be $11.75 \times 10^{19}\ (\mathrm{eV.sec.cm^3})^{-1}$ at x$\sim$0.69 and wavelength 324 nm, and the material gain has maximum values of order $5.671 \times 10^4\ \mathrm{cm^{-2}}$ for TM and $3.743 \times 10^7$for TE modes, respectively. Whenever the barrier is changed to ZnO, the results are different; at x~0.438 and wavelength 365 nm, the spontaneous emission becomes $2.965 \times 10^{19}\ (\mathrm{eV.sec.cm^3})^{-1}$ and the gain has maximum values of order $2.118 \times 10^4 \mathrm{cm^{-2}}$ for TM and $1.242 \times 10^5 \mathrm{cm^{-2}}$for TE mode.

Keywords: quantum dot, Spontaneous emission, Material gain, Wet layer, Barrier

1. Introduction

Quantum dot (QD) are nanostructures which have full quantization in all directions. This leads to distinct energy states, just like in real atoms, which enhances their optical spectrum. As a result, several studies on nanocrystals and their electro-optic properties have been performed [1-3]. Colloidal QDs, for example, have a broadening absorbance and are employed in solar cell and semiconductor optical amplifiers (SOA) application [4-6]. In addition to the core-shell structure's lattice matching, other factors that affect the distribution of quantized energy states in epitaxial grown core-shell QDs include the mole-fraction [6,7], and barrier type [8]. This makes it possible to control the band-gap of QD structures. In some cases, the emission spectrum's range can be extended from ultraviolet (UV) to near-infrared. Optical gain is the crucial factor in comprehending the behavior of QD semiconductor devices. When more input signal is added, gain maximum occurs [7]. Generally, UV may successfully stimulate semiconductor QDs with a broad absorption band. As a result, colloidal QDs appear to be appropriate for applications like as; colloidal quantum dot solar cells (QDSCs) [9]; white light-emitting diodes (WLEDs) [10]; applications in bioscience [11]; and quantum computing [12]. However, compounds II–VI have been the subject of much research in recent years for applications in the solar, electronic, photosensitivity, and semiconductor areas [13-17]. There has been a lot of interest in CdSe QDs (II-VI semiconductors). The possible use of CdSe QDs in light emitting devices in the yellow, blue, green and ultraviolet (UV) spectral regions is the big factor of the material's high level of interest. By using a unique design and custom known as a core/shell structure, in which a CdSe core is paired with a larger band-gap material like ZnS (around 12%) [18] and ZnO (around 7.1%) [19] where there is a slight lattice mismatch between them, CdSe semiconductor QDs can employed in various physical, chemical, and medicinal applications. The main objective of the current investigation is on the enhancement of spontaneous emission and material gain for the CdSe structure.

2. Methodology

2. 1. Optical energy band-gap of CdSe QDs

In this work, we started by evaluating the colloidal QDs' composition-dependent optical gaps for the system of

Cd(Se1-xSx) alloy. This system was used as an example of one that displays minor band-gap bowing (b). The following processes were used to determine the bulk semiconductor's energy band-gap (Eg), the effective mass of electrons and holes ($\boldsymbol{m_e^*}$ and $\boldsymbol{m_h^*}$),respectively, parameters used in the computation, along with a pseudo-binary alloyed system, such as ABxC1-x, i.e., is determined by the following appropriate relationships [20]

$$E_g(x) = xE_g(AB) + (1-x)E_g(AC) - b(1-x)x, \quad (1)$$

when the unalloyed compounds AB and AC's respective energy band gaps are Eg(AB) and Eg(AC). The following equation for the ABxC1-x alloyed system provides the effective mass of the structure at x-compositions [19,20]

$$m(x) = xm(AB) + (1-x)m(AC)\,, \quad (2)$$

where the effective mass of the unalloyed semiconductors compounds of AB and AC, respectively, are symbolic by $m^*(AB)$ and $m^*(AC)$. Table.1 shows the bowing parameter (b), the energy bandgap of the bulk semiconductor (E_g) and the effective mass of the electrons and holes (m_e^* and m_h^*), respectively [20 - 25].

2. 2. Quasi-Fermi energy states, the material gain, and spontaneous coefficient

In order to account for the form defects and random distributions in the QDs through their formations, it is necessary to consider the broadening of the QDs spectrum as a result of inhomogeneity. Consequently, the material gain and spontaneous emission coefficients could both be defined via [2]

$$g_\sigma^{trans}(\hbar\omega) = \frac{\pi e^2}{n_b c \varepsilon_o m_o^2 \omega^2} \sum_i \int dE' \, |M_{env}|^2 P_{trans}^2 D(E') L_g(E', \hbar\omega) F_\sigma, \quad (3)$$

The expression "σ" can either refer to the gain (α) or the spontaneous emission (sp). Considering gain;

$$F_\alpha = f_c(E', F_c) - f_v(E', F_v), \quad (4)$$

Likewise, when spontaneous emission happens [26,27]

$$F_{sp} = f_c(E', F_c)[1 - f_v(E', F_v)]\,, \quad (5)$$

The symbols f_c and f_v, respectively, are denote to the Quasi-Fermi functions for the conduction and valence bands, while the conduction and valence bands' equivalent Quasi-Fermi energies are F_c and F_v, respectively. The global Quasi-Fermi levels, which are formed by the WL and QD contributions, must be taken into consideration for accurate calculations. The electron-heavy hole energy momentum matrix element ($\vec{p}_{trans}$) can be calculated as follows.

Subscript (trans) indicate that the mode is either TE or TM. For the electron-heavy hole transition energy in the TE mode [28], the momentum matrix element is defined as

$$|\hat{e}.\vec{p}_{cv}|^2|_{TE} = \frac{3}{2}(m_o/6)E_{p,} \quad (6)$$

while for TM mode case is given by [29];

$$|\hat{e}.\vec{p}_{cv}|^2|_{TM} = \frac{3}{2}\left(1 - \frac{E_{cym}}{E_{cnml}}\right) \times (m_o/6)E_{p,} \quad (7)$$

where, E_{cym} is the energy of a conduction subband in the y-direction, while the QD state's E_{cnml} is that. The parameter, E_p is the optical matrix energy. Others scripts in Eq. (3), n_b, ε_o, c, m_o and M_{env}, are the material background refractive index, permittivity's of free space, the light speed, the electrons' free mass, the envelope function of the QD electrons and holes states. $D(E')$ is the self-assembled QDs' inhomogeneous state density and is defined by [2]

$$D(E') = \frac{s^i}{V_{dot}^{eff}} \frac{1}{(2\pi\sigma^2)^{1/2}} \exp\left(\frac{-(E' - E_{max}^i)^2}{2\sigma^2}\right), \quad (8)$$

s^i is the degeneracy number at each QD state, where $s^i = 2$ for the ground state and $s^i = 4$ for the excited state. The parameters V_{dot}^{eff}, σ, and E_{max}^i are effective volume of QDs, spectral variations of the QDs distribution, the maximum transitional energy, respectively. The equation for the Gaussian line shape function ($L_g(E', \hbar\omega)$) which is applied for the material gain with a linewidth variance (γ), follows [2]

$$L_g(E', \hbar\omega) = \frac{1}{(2\pi\gamma^2)^{1/2}} \exp\left(\frac{-(E' - \hbar\omega)^2}{2\gamma^2}\right), \quad (9)$$

Furthermore, from the surface carrier density per QD layer for electrons (n_{2D}) and holes (p_{2D}), and both the QDs and WL contributions are taken into account, the following equations can be used to numerically calculate the Quasi-Fermi levels of the conduction band F_c and valence band F_v [2]

$$n_{2D} = N_D \sum_i \frac{s^i}{\sqrt{2\pi\sigma_e^2}} \int e^{-(E_c' - E_{ci}^D)^2/2\sigma_e^2} f_c(E_c', F_c)\, dE_c' + \sum_l \frac{m_e^W k_B T}{\pi\hbar^2} \ln\left(1 + e^{(F_c - E_{el}^W)/k_B T}\right) + t_B \int \frac{1}{2\pi^2} \left(\frac{2m_e^B}{\hbar^2}\right)^{3/2} \sqrt{(E_c' - E_c^B)} f_c(E_c', F_c)\, dE_c'\,, \quad (10)$$

$$p_{2D} = N_D \sum_j \frac{s^j}{\sqrt{2\pi\sigma_h^2}} \int e^{-(E_h' - E_{hj}^D)^2/2\sigma_h^2} f_v(E_h', F_v)\, dE_h' + \sum_m \frac{m_h^W k_B T}{\pi\hbar} \ln\left(1 + e^{(F_v - E_{hm}^W)/k_B T}\right) + t_B \int \frac{1}{2\pi^2} \left(\frac{2m_h^B}{\hbar^2}\right)^{3/2} \sqrt{(E_h^B - E_h')} f_v(E_h', F_v)\, dE_h'\,, \quad (11)$$

where N_D is the QD density, E_c' and E_h' are the conduction and valence band energies, respectively. E_{ci}^D and E_{hj}^D are the respective confined QD state in the conduction and valence bands, respectively. σ_e and σ_h are the spectral variance of electrons and heavy-holes distributions in QDs, respectively. k_B is the Boltzmann constant and T is the QD temperature. The $m_e^W(m_h^W)$ are the effective electrons (holes) masses and E_{el}^W (E_{hm}^W) are the subband edge of the conduction (valence) band of wetting layer (w). The t_B is the thickness of the barrier in each layer of QDs. While, terms m_e^B (m_h^B) and E_c^B (E_h^B) are the carriers masses and the band edge of the conduction (valence) band of the barriers layer. Also, f_c and f_v are quasi-Fermi distribution function for the conduction and valence bands, respectively. It's given by [2]

$$f_c(E_c', F_c) = \left[1 + \exp\left[(E_g + E_{ei} + \left(\frac{m_r^*}{m_e^*}\right)(E_c' - E_{hi}^{ei}) - F_c)/K_B T\right]\right]^{-1}, \quad (12a)$$

$$f_v(E_h', F_v) = \left[1 + \exp\left[(E_{hi} - \left(\frac{m_r^*}{m_{hh}^*}\right)(E_h' - E_{hi}^{ei}) - F_v)/K_B T\right]\right]^{-1}, \quad (12b)$$

The term E_g is the energy bandgap of QD. The discrete confined energy states of QD in the conduction and valence bands are termed as E_{ei} and E_{hi}, respectively. While, the transition between the energy of QD states in

the conduction and valence bands is defined E_{hi}^{ei} $(= E_g + E_{ei} - E_{hi})$. m_e^* , m_{hh}^* and m_r^* $(= \frac{1}{m_e^*} + \frac{1}{m_{hh}^*})$ are the effective electron and heavy-hole masses. On the otherhand, the spontaneous emission rate, R_{sp} is defined as is characterized as a numbers of photon released per second per unit volume per unit energy, and it's given by [2,28,29]

$$R_{sp} = \frac{n_r^2 w^2}{\hbar \pi^2 c} \frac{(2.g^{TE} + g^{TM})}{3}. \quad (13)$$

3. Results and discussion

In Table.1, the data that were used in the computations are listed. Results of the CdSe/CdS QD structure are described in this section and are grouped once according to the type of barrier (ZnS or ZnO) and again according to the composition (x). This study explores zinc blende (ZB) CdSe-containing structures because ZB is metastable under normal situations [9]. Eqs. (1) and (2) for ternary semiconductor systems are used to determine the structures initially, and all accord with table 1. Using the bow parameters described in Table 1, Eqs. (1) and (2) calculate the bandgap and effective mass of the structures. The linewidth variance (γ) and spectral variance (σ), which appear in Eqs. (8)–(12), are considered to be $(0.05\ eV)$, and $N_D\ = 5 \times 10^{14} m^{-2}$ for the density's QD, and $n_{2d}\ = 2 \times 10^{14} m^{-2}$ for surface carrier [2], the simulation is carried out. The quantum disks shape being researched in this study are considered to have a radius of $(\rho = 15nm)$ and a height of $(h = 3nm)$. By dividing the issue into two problems: the inplane (ρ-φ) and the issues with Z-direction, the Schrodinger equation for the quantum disk in cylindrical dimensions is used to predict the QD energy levels. The energy levels are then computed using the boundary conditions between the barrier and QD active regions. References [1,2] describe this type of issue in detail. The predicted energy levels are compared to the results of studies in Refs. [2,30].

After inserting the surface carrier density by Eqs. (10) and (11), estimates are prepared for the Fermi-energy levels and, therefore, the Fermi function. Furthermore, the material gain is calculated for the TE (using Eq.(6)) and TM (using Eq.(7)) modes using Eq.(8) and Eq.(9), respectively, which incorporate $D(E')$ and $L_g(E', \hbar\omega)$ using Eq.(3). Thus, the spontaneous coefficients are obtained by using Eq. (14) as a total of gain for the TE and TM modes. Table 1 is used as a mole-fraction-dependent parameter to calculate the material gain and the spontaneous emission coefficient of the QD structures using Eqs. (1) and (2).

3. 1. CdSe/ZnS structures

The TE and TM gain modes in figure 1 illustrate the structure in the QD region at four x-mole fractions (from 0.690 to 0.693). First, consider well about revisions in the mole fraction (~ 0.001) shown in table 2, which dramatically influence the spectra by shifting the bandgap energy. The TE spectra have the same form as the TM spectra but are three orders higher. The peak of each spectrum is at 324.2 nm. The gain is reduced by more than one order when the x-mole fraction of CdSe is reduced. The gain spectra are given by the spontaneous emission spectra.

In contrast to its quantum well (QW) counterpart, high TE (and TM) is important for LED applications and it seems promising especially UV LED with QD. The results indicate that the optical transition between the QD energy subband is just what influences the peak wavelength position. For $CdSe_{.310}S_{.690}$ structure, Quasi-Fermi energy in the conduction band is $F_c = 2696.8$ MeV, which is upper-lying overall the conduction subband of QD, and Quasi-Fermi energy in the valence subband is $F_v = -888.0$ MeV, which is lower-lying overall the valence subband of QD, whereas that of $CdSe_{.307}S_{.693}$ structure, $F_c = 2700.5$ and $F_v = -745.6$ MeV. Most carriers in these states can then take part in advantageous transitions, resulting in a significant material gain. The difference in Quasi-Fermi levels for $CdSe_{.310}S_{.690}$ structure is $\Delta F_{cv} = 3584.8$MeV, while for $CdSe_{.307}S_{.693}$ structure is $\Delta F_{cv} = 3446.1$ MeV. Furthermore, the CdSe QD region's bandgap energy is 1588.2 MeV for the $CdSe_{.310}S_{.690}$ structure compared to 1591.0 MeV for the $CdSe_{.307}S_{.693}$ structure. According to these results, the QD's energy bandgap and Fermi-energy difference of the $CdSe_{.310}S_{.690}$ structure are wider by 2.8 MeV and 138.7 MeV, respectively.

3. 2. CdSe/ZnO structures

By changing the barrier layer (ZnO), one can get to the conclusion that the QD structure with the higher gain has a smaller energy QD-bandgap. Figure 2 shows the change barrier (ZnO) effects on the CdSe(1-x)S(x) structure. Through considering the effects of changing ZnO-barrier layer at four x-mole fractions (from 0.438 to 0.4395), the structure of the CdSe-QD can be investigated. The TE and TM gain spectrum are more than three times lower with the ZnO-barrier layer included, and the peak wavelength in figure 2 is (42 nm) UV-shifted from figure 1 This shift in wavelength may indeed be attributed to the ZnO presence in the CdSe(1-x)S(x) structure, which leads the difference barrier band-gap energy to decrease to 3147.2 MeV.

4. Conclusion

Theoretically, UV-emitted CdSe barrier-based QD structures are The ternary structure i.e. CdSe(1-x)S(x), lattice-matched systems, are being investigated. Spontaneous emission occurs in these structures, along with TE and TM gain spectra. The gain spectra also be seen in the spontaneous emission spectra. For the barrier ZnO-containing structure, the spontaneous emission coefficient is dropping. At wavelength 365.5 nm, a peak appears in all of the structure's spectra with a ZnO barrier. Gain may be enhanced by either increasing the x-composition in the QD active region or at the barrier region, replacing ZnS. It is important for UV technological applications that such range of ΔE_g in UV be extended from 1373 to 1591 MeV.

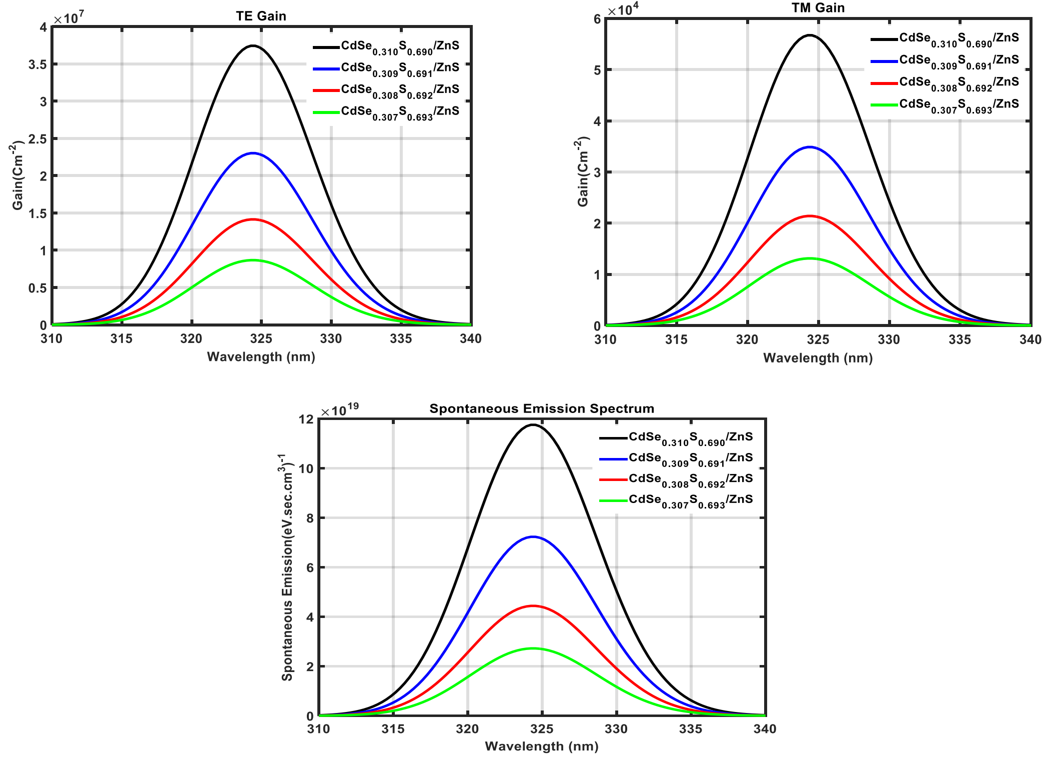

Figure 1. For the CdSe/ZnS QD structure: TE and TM gain and the spontaneous coefficient.

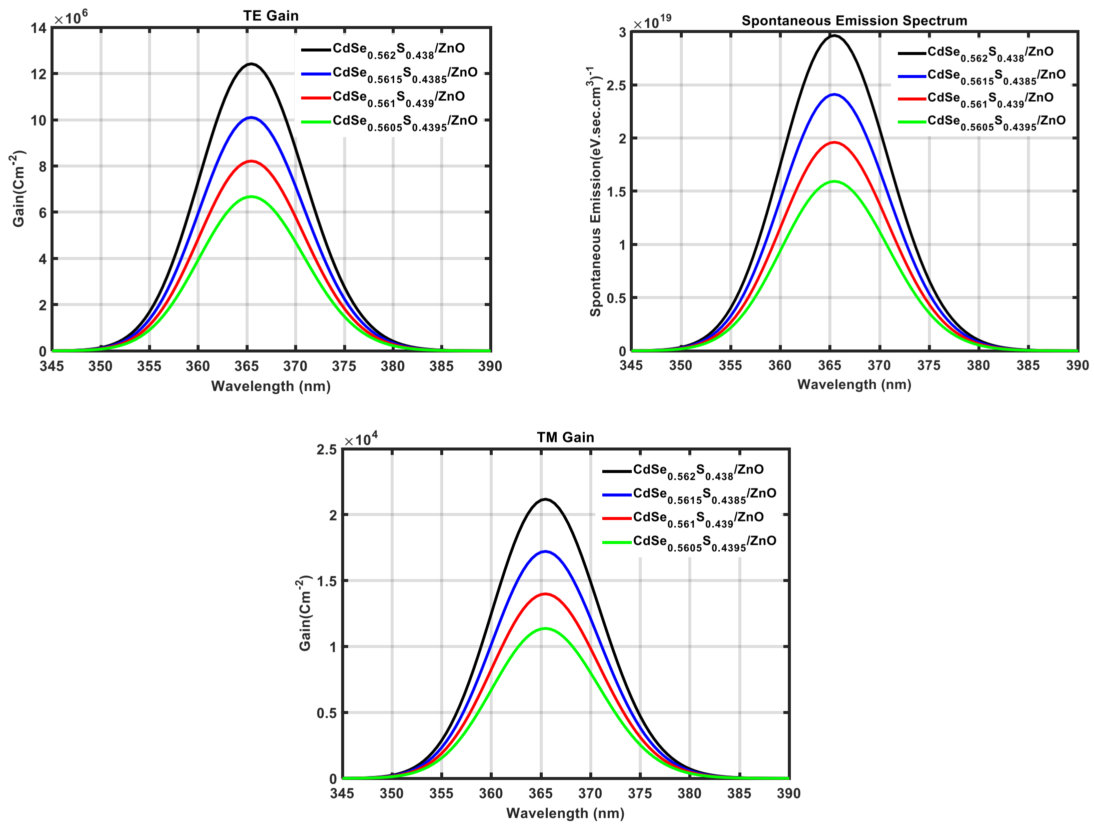

Figure 2. For CdSe/ZnO QD structure: TE and TM gain and the spontaneous coefficient.

Table 1. The experimental data for E_g, m_e, m_h, and b that were used in computations.

Par.	CdSe	CdS	ZnO[26]	ZnS
m_e^*/m_0	0.13	0.140	1.88	0.39
m_h^*/m_0	0.45	0.51	2.90	1.76
Eg / eV	1.74	2.55	3.37	3.83
b / eV	0.28	-	-	-

Table 2. Summary of the predicted gap ΔE_g $(= E_{gB} - E_{gQD})$ between the barrier's bandgap and the QD region's bandgap, the Quasi-Fermi energy levels difference ΔF_{cv} $(= F_c - F_v)$, the peak wavelength for TE and TM transition modes (λ_{p-TE}, λ_{p-TM}), respectively, and the peak material gain for TE and TM transition modes (g_{p-TE}, g_{p-TM}), respectively, for the structures under study.

Structure	ΔE_g (MeV)	ΔF_{cv} (MeV)	λ_{p-TE} (nm)	λ_{p-TM} (nm)	g_{p-TE} (m^{-2})	g_{p-TM} (m^{-2})
$CdSe_{.310}S_{.690}/ZnS$	1591.0	3584.8	324.2	324.2	3.743×10^7	5.671×10^4
$CdSe_{.309}S_{.691}/ZnS$	1590.1	3444.5	324.5	324.5	2.302×10^7	3.486×10^4
$CdSe_{.308}S_{.692}/ZnS$	1589.2	3445.3	324.5	324.5	1.413×10^7	2.139×10^4
$CdSe_{.307}S_{.693}/ZnS$	1588.2	3446.1	324.2	324.5	0.8665×10^7	1.311×10^4
$CdSe_{.562}S_{.438}/ZnO$	1374.1	3147.2	365.5	365.5	12.42×10^6	2.118×10^4
$CdSe_{.5615}S_{.4385}/ZnO$	1373.8	3146.9	365.5	365.5	10.1×10^6	1.722×10^4
$CdSe_{.361}S_{.439}/ZnO$	1373.4	3147.1	365.5	365.5	8.214×10^6	1.40×10^4
$CdSe_{.5605}S_{.4395}/ZnO$	1373.0	3147.5	365.5	365.5	6.676×10^6	1.137×10^4

References

1. J Jamal, M Sabah, and A Amin, *J. Phys. Conf. Ser.* **1234** (2019) 012019.
2. J Kim and S L Chuang, *IEEE J. Quantum Electron* **42** (2006) 9.
3. B Al-Nashy, S Razzaghi, M Al-Musawi, S Rasooli, and A Amin, *Results in Physics* **7** (2017).
4. D Tahseen, A M Samir, and A Amin, *Appl. Opt.* **57** (2018).
5. D Tahseen, A M Samir, and A Amin, *Micro Nano Lett.* **13** (2018).
6. M Al-Mossawi, A Al-Shatravi, and A Al-Khursan, *Insciences J.* **2** (2012) 2.
7. A Al-Shatravi, B Al-Nashy, and A Al-Khursan, *Journal of Optical Communications* (2020).
8. J Jamal, M Sabah, and A Al-Khursan, *Plasmonics* **14** (2019).
9. M Albaladejo, C Elizabeth, D Koch, L Yanxiu, A Rogach, and Y Vaynzof, *Adv. Energy Mater* **11** (2021) 12.
10. H Chen, H Cheng, and H Hong, *IEEE Photonics Technology Letters* **18** (2006) 1.
11. N Bajwa, N Mehra, K Jain, and N Jain, *Biotechnol* **44** (2015) 3.
12. L Vandersypen and M Eriksson, *Physics Today* **72** (2019) 8.
13. L Yitan, W Lin, W Cuncun, L Chang, Y Chen, L Hong, J Jun, and M Liangmo, *J. Mater. Chem. A* **2** (2014).
14. O Olusola, O Echendu, and I Dharmadasa, *Journal of Materials Science: Materials in Electronics* **26** (2015).
15. P Chauhan, A Patel, S Narayan, J Prasad, C Sumesh, G Solanki, K Patel, S Soni, P Jha, V Pathak, and V Patel, *Journal of Alloys and Compounds* **862** (2020).
16. S Hussain, M Iqbal, A Khan, M Khan, G Mehboob, S Ajmal, M Ashfaq, G Mehboob, M Ahmed, S Khisro, C Li, R Chikwenze, and S Ezugwu, *Front. Chem.* **9** (2021).
17. K Sediq, *ARO* **9** (2021) 2.
18. J Llusar, J Planelles, and J Climente, *The Journal of Physical Chemistry C* **123** (2019) 34.
19. A Erin, J Monique, A Jasmin, and K Aswini, *A Potential Sensing Platform* **1** (2021).
20. H Asano and T Omata, *AIP Advances* **7** (2017).